***TITANS***

*Research and Innovation Action (RIA)*

Funded by the European Union. Views and opinions expressed are however those of the author(s) only and do not necessarily reflect those of the European Union or the European Atomic Energy Community ('EC-Euratom'). Neither the European Union nor the granting authority can be held responsible for them.

Start date : 2022-10-01 Duration : 36 Months

# Improvement of tritium measurement techniques

Authors : Dr. Kimberly COLAS (CEA), J. Bubendorff, R. Laumonier, Y. Kergadallan, C. Gautier, P. Fichet, T. Charpentier, A. Listwan, M. Moskura, O. Debellemanière, M. Payet, G. Dougniaux, S. Peillon (CEA Paris-Saclay, France) S. Markelj, M. Kelemen, E. Punzon-Quijorna, M. Lipoglavsek, A. Cvetinovic, P. Pelicon (Jozef Stefan Institute , Slovenia) A. Bultel, A. Favre, V. Morel (Coria, UMR 6614, CNRS-Normandie Université-INSA de Rouen, France) E. Bernard (CEA-Cadarache, France)

TITANS - Contract Number: 101059408

Project officer: Angelgiorgio Iorizzo

| | |
|---|---|
| Document title | Improvement of tritium measurement techniques |
| Author(s) | Dr. Kimberly COLAS, J. Bubendorff, R. Laumonier, Y. Kergadallan, C. Gautier, P. Fichet, T. Charpentier, A. Listwan, M. Moskura, O. Debellemanière, M. Payet, G. Dougniaux, S. Peillon (CEA Paris-Saclay, France) S. Markelj, M. Kelemen, E. Punzon-Quijorna, M. Lipoglavsek, A. Cvetinovic, P. Pelicon (Jozef Stefan Institute , Slovenia) A. Bultel, A. Favre, V. Morel (Coria, UMR 6614, CNRS-Normandie Université-INSA de Rouen, France) E. Bernard (CEA-Cadarache, France) |
| Number of pages | 35 |
| Document type | Deliverable |
| Work Package | WP02 |
| Document number | D2.1 |
| Issued by | CEA |
| Date of completion | 2024-07-25 09:56:23 |
| Dissemination level | Public |

**Summary**

The document describes a review of the different techniques available to analyse tritium, commercially developed and/or published. Tritium is a very difficult radionuclide to analyse. Many different techniques to measure tritium are encountered in the literature with varying precisions and possible applications. R&D is still required to improve methods to analyse tritium. This document corresponds to the deliverable D2.1 of the TITANS project.

Approval

| Date | By |
|---|---|
| 2024-07-25 10:06:08 | Dr. Moreno CARLOS (CIEMAT) |
| 2024-07-26 12:16:14 | Mrs. Elodie BERNARD (CEA) |

# Disclaimer

Funded by the European Union. Views and opinions expressed are however those of the author(s) only and do not necessarily reflect those of the European Union or the European Atomic Energy Community ('EC-Euratom'). Neither the European Union nor the granting authority can be held responsible for them.

# Table of Contents



# List of Figures



Funded by the European Union

Funded by the European Union

## List of Tables



Funded by the European Union

# Abbreviation and Acronyms

| Acronym | Description |
|---|---|
| AMS | Accelerator mass spectrometry |
| FCM | Full combustion method |
| LIBS | Laser-Induced Breakdown Spectroscopy |
| LTE | Local Thermodynamic Equilibrium |
| MAS | Magic-angle spinning |
| MKPc | Magnesium potassium phosphate cement |
| NMR | Nuclear Magnetic Resonance |
| NRA | Nuclear Reaction Analysis |
| RANS | Reynolds-averaged Navier–Stokes |
| SiPM | Silicon Photomultipliers |
| WP | Work package |

# Introduction

The document describes a review of the different techniques available to analyse tritium, commercially developed and/or published. Tritium is a very difficult to analyse radionuclide. Many different techniques to measure tritium are encountered in the literature with varying precisions and possible applications. R&D is still required to improve methods to analyse tritium. This document corresponds to the deliverable D2.1 of the TITANS project.

Funded by the European Union

# 1 Tritium measurement using autoradiography

Autoradiography is a technique able to measure the electron emitted during the decay of tritium. It provides an image of the distribution of radioactivity of the surface/sub-surface of the sample since the mean free path of an electron of 16 KeV is rather limited in metal materials. Autoradiography using SiPMs (Silicon Photomultipliers) developed at CEA Saclay laboratory (LASE) is a fast (3 minutes) and flexible technique dedicated to difficult to measure radionuclides (particularly tritium but also alpha). During TRANSAT it was clearly proven that Autoradiography with SiPM can be used to assess the amount and the homogeneity of tritium on Tungsten (W) surface. Some samples were prepared during the TRANSAT program to evaluate the feasibility of preparing stable tritium sources as well as samples that can be shipped without travel authorization due to their low activity. This last point is essential to compare different techniques. Today the autoradiography system is a mobile system that can perform measurement at decommissioning sites.

During the tritium school that took place in June of 2021, it was clearly explained the needs of an ideal technique to investigate tritium: sensitive, stable, no tritium memory effect, providing tritium depth (at a scale of few micrometers). No such technique exists today. Autoradiography with SiPM was developed mainly for alpha emitters. However, for beta emitters, many parameters must be improved: the scintillator (type, thickness), the type of SiPM (different models), the electronic part. Currently, the response of the electronic can be greatly improved to lower the detection limit and to broaden the resolution in terms of photon counting. This last point is essential to separate the response of alpha and beta emitters.

An autoradiography system with SiPM was developed during TRANSAT-1 to be useful to all kinds of investigation of solid matrices as well as tritiated particles. In the framework of tritiated waste studies autoradiography could be a relevant solution in terms of decision to find free release solution (as an example analysis of smears).

To achieve a very sensitive measurement, the development has been pushed towards a demonstrator with an active detection area in direct contact with the potential contaminated solid surface. Removing the use of any protective window increases the detection capability, compared to existing contamination monitors, but causes additional constraints. To meet these requirements, the detection was based on organic scintillators coupled with SiPM (Silicon PhotoMultiplier) arrays, which were used to collect the light emitted when a radiation is going through the scintillator.

Funded by the European Union

Organic scintillators are widely used for charged particles detection, are robust to mechanical constraints and are fairly easy to clean. The detection system built is based on four independent Hamamatsu SiPM arrays each containing 16 independent SiPM in close contact. A total of 64 (4*16 SiPM) can be used with the new demonstrator. Above each array a plastic scintillator is placed (3 mm thick, a square of 5 cm * 5 cm) without any use of optical coupling grease/glue.

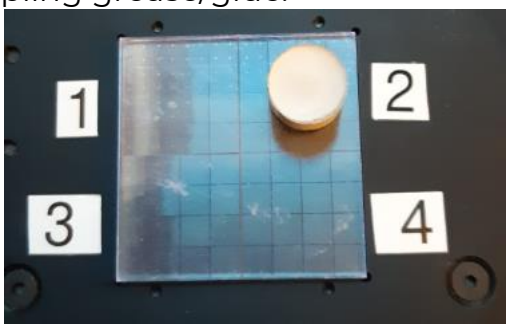


**Figure 1: SiPM demonstrator containing 64 independent SiPM (as an example a sample mad of concrete is placed in one SiPM array). The size of the sensitive part is 5 cm* 5 cm.**

Each array is composed of 16 independent cells of individual size of 6 x 6 $mm^2$. The readout of the 64 channels was performed using a dedicated ASIC, a FPGA and a 16 bits ADC. The system was supplied by a power supply which provides, in addition to the bias voltage (of the order of 54V), a valuable real time read-out of the current going through the SiPM arrays (typically at the µA level). All the components of the demonstrator have been enclosed in an airtight black box to ensure proper light insulation when the device is started. During the experiment, the prototype was also connected to a computer using a USB cable and the data acquisition was controlled using a dedicated software developed by the Laumonier company (France, in charge of the commercial developments of the MAUD system for dismantling applications).
The SiPM device is a photon detector and by using a plastic scintillator, the SiPM locally records photons induced by the radioactivity (for TRANSAT, tritium). When the amplitude signal of any of the 64 SiPM exceeds the detection background, the data acquisition is triggered and the computer records the corresponding ADC value of all the 64 SiPMs cells. A SiPM provides an analog output signal with amplitude proportional to the number of detected photons by the cell.
During each individual measurement, the tritium sources were placed in direct contact with the scintillator, which was placed on top of SiPM arrays. As it was previously mentioned, the tritium sources are very difficult to prepare. The tritium sources were prepared at French Alternative Energies and Atomic Energy Commission (CEA), Saclay via hydrogen isotope gas charge at elevated temperatures. The matrix chosen is W to ensure the stability of the tritium trapped on the surface (Bernard, 2019). Values considered for these solid sources correspond to similar samples prepared

in the same way but analysed by a destructive technique (Pyrolysis + LSC (Liquid Scintillation Counting). The acquisition time was set at 3 minutes, typical duration for field measurement in nuclear facilities.
By using each signal coming from the 64 SiPM, some kind of image reconstruction was calculated by the software. The image reconstruction has proved the applicability of the system, its sensitivity and ability to observe locally the radioactivity.
Figure 2 highlights the first measurement obtained on a tritium source. This tritium sample corresponds to a tungsten (W) matrix with a whole quantity of tritium measured at 220 MBq/g (with LSC measurement after pyrolysis). The image reconstruction corresponds in orange and red to the localization of the source. The green colour corresponds to SiPM at background level. With 220 MBq/g, the signal versus background ratio of the “hot point” can be estimated at 158624/200 ≅ 800. This source is easily distinguished from the background. The sensitivity of the system is not easy to assess because MAUD can only measure for tritium, radioactivity coming from the surface and the measurement of 220 MBq/g corresponds to the whole tritium measurement.

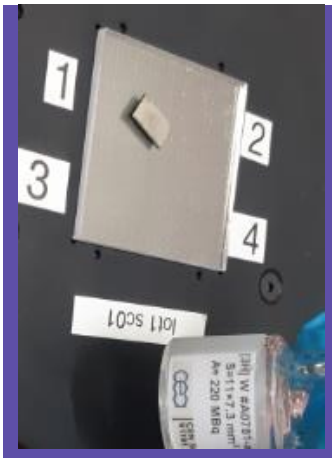


**Sample on SiPM array 1**

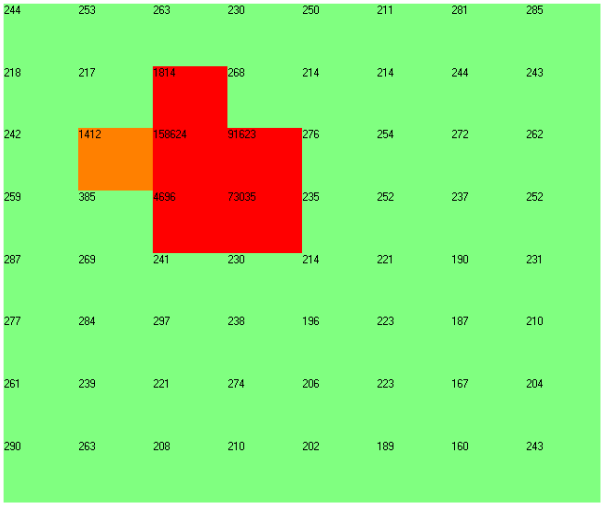


**Figure 2: Left the sample deposited on the MAUD surface, Right image reconstruction after the acquisition.**

Another W matrix containing tritium estimated at 50 000 Bq/cm$^2$ (evaluated by the CEA team that prepared the sample) was also measured by MAUD demonstrator (Figure below for the polished surface).

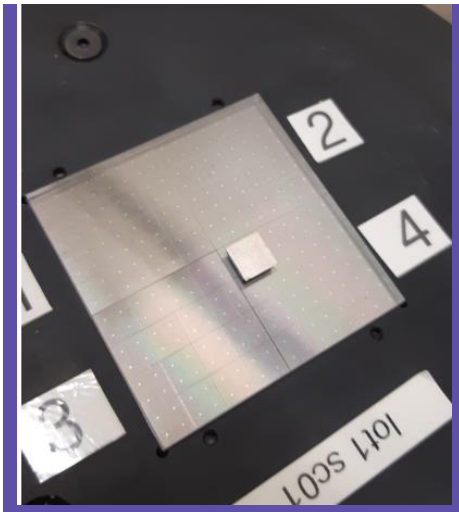


**Sample on SiPM array 4**

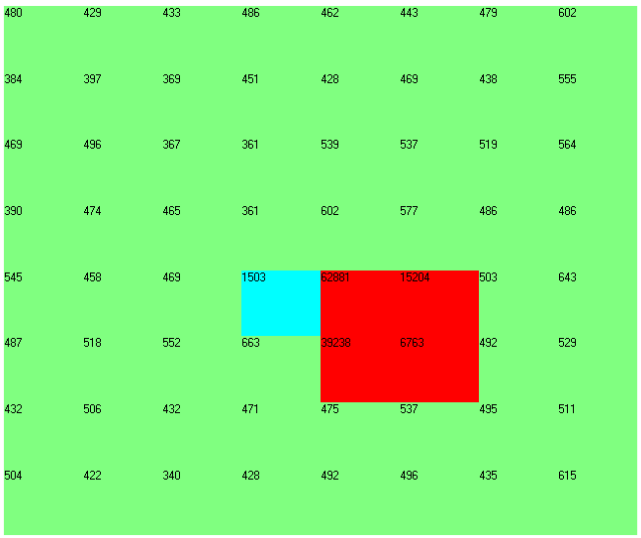


Maximum trigger at 62881

**Figure 3: Left the sample (polished surface) deposited on the MAUD surface, Right image reconstruction after the acquisition.**

Figure 4 corresponds to the same sample but in the other side (non-polished surface).
It can be concluded that the amount of tritium on the polished surface is less important than in the unpolished surface.

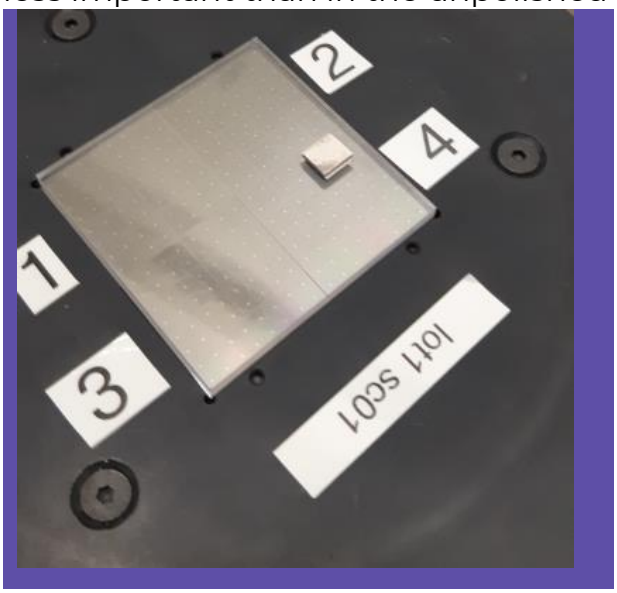


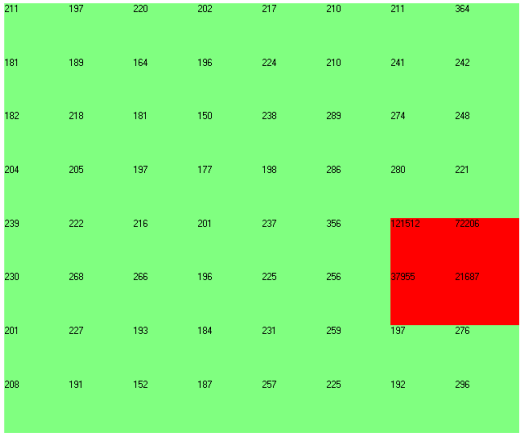


Maximum trigger at 121512

**Figure 4: Left: the sample (unpolished surface) deposited on the MAUD surface, Right: image reconstruction after the acquisition.**

Before and after all these measurements, acquisitions without sample on the MAUD system were recorded. Figure 5 shows the reconstruction of the background image. This proves that no tritium memory effect was observed after all the measurements.

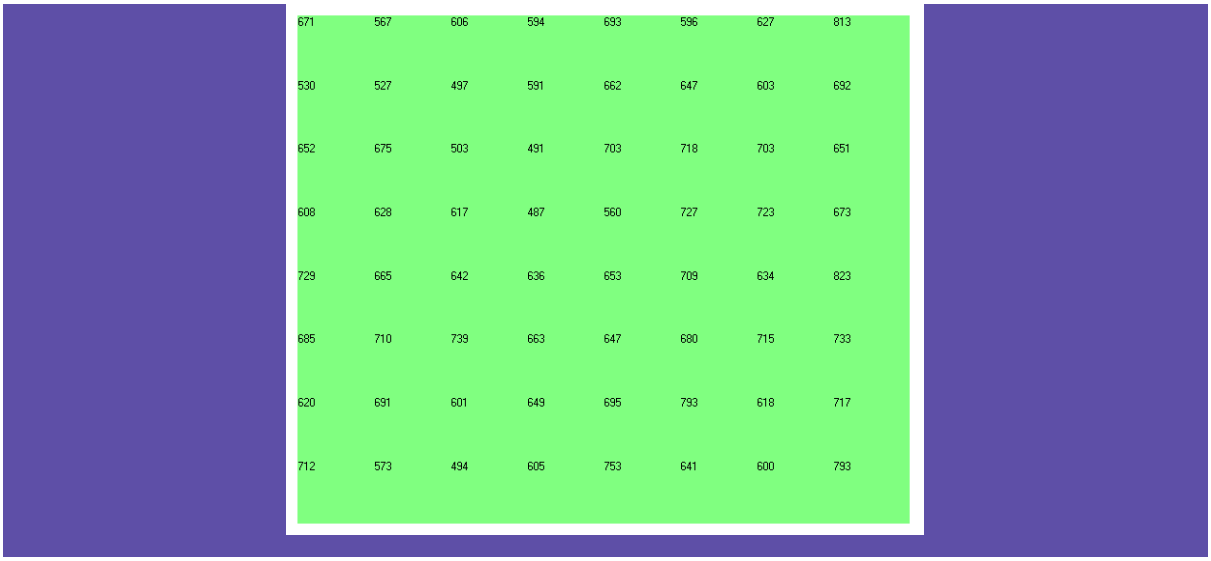


**Figure 5: image reconstruction after the acquisition of the background after acquisition of all the tritiated sources tested.**

As described, it was very difficult to prepare many tritium sources during TRANSAT, which still remains very challenging. However, during the developments of the demonstrator, it was demonstrated that both for alpha and beta emitters, the detection response is sufficiently linear to perform a real time contamination estimation. The autoradiography device with SiPM is able to record tritium activity coming from the surface. With the ARC source (see Figure above) a detection limit of 100 Bq/cm$^2$ was determined. These first results are very encouraging for the tritium measurements for which no industrial solution can currently be found to investigate this radionuclide on solid surface. To enlarge the measurement with SiPM, the system can be easily connected with a robot.
The distribution of the photons recorded for tritium radionuclides and for different other alpha or beta nuclides is different, which may be interesting in the use of SiPM demonstrator. The SiPM system can be useful for fission or fusion measurements.

Recent development has been performed within the collaboration framework between CEA and Atelier Laumonier which is now the manufacturer of the MAUD system. A version, usable in laboratory as well as directly in contact with the surface has been developed as represented in the following figure.


**Figure 6 MAUD system for in laboratory measurement and surface measurement**

However, new needs for measurement of tritium in various surface require a large number of measurements to be made and thus have led to the modification of this system. The newly developed system is capable of being used for large surfaces as well as on walls and door frames. This system is more portable is more user friendly and can be seen in the following figure.


**Figure 7 Modified MAUD system for measurement of large surfaces.**

Funded by the European Union

Tests are planned in areas where tritium (and carbon 14) are known to have migrated and contaminated various surfaces using the new system during the 2024 year.

# 2 Development of Nuclear Magnetic Resonance for measuring tritium in solids

## 2.1 NMR principles and isotopes of interest

Solid State Nuclear Magnetic Resonance is a spectroscopy which probes the local environment of atoms using the radio-frequency signal (called free induction decay or FID) emitted by nuclear spins **I** when placed in a constant magnetic field $B_0$. The magnetic moment of nuclei ($\vec{\mu} = \hbar\vec{I}$) are excited by a strong short radio-frequency pulse (typically few µs of length) resonant with their Larmor frequency $\nu_L$defined as $\nu_L = -\gamma B_0$ where $\gamma$ is the gyromagnetic ratio, a property specific of the isotope studied. The higher is the Larmor frequency, the higher is the NMR sensitivity. Hydrogen possesses three NMR active isotopes (i.e., with a non-zero nuclear spin **I**) which are reported in Table 1. Tritium $^3$H is the most sensitive NMR element of the periodic table, slightly above protium $^1$H which is ubiquitous in materials science. As the decaying product of tritium (half-time 12.44 years), helium-3 $^3$He is also a sensitive nucleus for NMR spectroscopy and can thus be considered as a potential probe for studying of tritiated materials (and their ageing). Helium-4 is not NMR-active because of its vanishing nuclear spin **I**=0.

| **NMR isotope** | Nuclear spin **I** | Natural abundance | Gyromagnetic ratio $\gamma$ (MHz.T$^{-1}$) | Larmor frequency $\nu_L$ (MHz) at $B_0$=11.72T |
|---|---|---|---|---|
| **protium $^1$H** | ½ | 99.9855% | 42.577 | 499.1 |
| **deuterium $^2$H** | 1 | 0.0145% | 6.536 | 76.6 |
| **tritium $^3$H** | ½ | trace | 45.414 | 532.2 |
| **helium-3 $^3$He** | ½ | 0.000134% | -32.434 | 380.1 |

**Table 1. NMR properties of the hydrogen isotopes (protium, deuterium and tritium) and helium-3. The Larmor frequency is given for the magnetic field used in our laboratory (Bruker Wide-Bore UltraShield Superconducting magnet 500WB, see Figure 8).**

Funded by the European Union

In addition to the Larmor frequency the NMR frequency contains contributions (perturbations under high-magnetic field conditions) arising from the *magnetic interactions* of the nuclear magnetic moment of the atom of interest with its surrounding. This is typically the chemical shift. In many solids however, the contributions from dipolar magnetic interactions between nuclear magnetic moments are generally dominant and detrimental to the spectral resolution (vide infra). The local magnetic interactions generate the NMR shift (given in ppm of $\nu_L$) that encodes the local environment of the atoms (i.e., its chemical speciation). After Fourier transform of the NMR signal, the NMR spectrum contains resonances that reveals each different local environments of the studied atoms. Additionally, dynamical information can be extracted from the NMR signal: life-time of the NMR signal and the return of the nuclear magnetization to its equilibrium along the magnetic field, encoded in the transverse relaxation times $T_2$ and longitudinal relaxation time $T_1$, respectively (Bloch equations). *One of the motivations for developing $^3H$ NMR is to determine the speciation of the tritium in solids with the help of measured NMR properties (NMR shift and relaxation times).*
Because of its very large palette of techniques and its versatility, [1][2][3] NMR has established itself as an important spectroscopy in many areas of biology, chemistry, physics and materials sciences, as most elements of the periodic have NMR active isotopes. Each atom can then be viewed as a probe of the local structure and dynamics, complementary to the other NMR active nuclei, thanks the isotopic selectivity of NMR (each isotope can be studied independently as Larmor frequencies are well separated from each other at standard high magnetic field values).

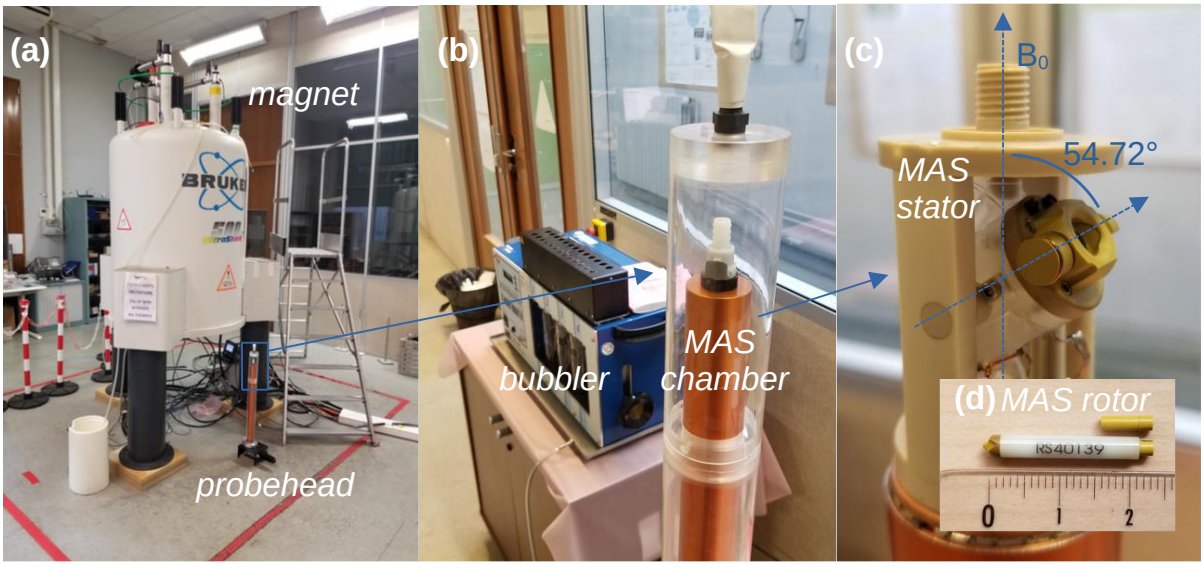


**Figure 8. Overview of the NMR laboratory were 3H NMR experiments are performed. (a) 500 Wide Bore superconducting magnet (operating at 11.72T) and one of the tritium MAS NMR probehead; (b) enlarged view of the probehead showing the connectors of the exhaust spinning gas to a tritium bubbler; (c) view of the MAS stator oriented at the magic-angle with respect to the magnetic field; (d) example of MAS rotor (3.2mm outer diameter; $ZrO_2$) with the top cap. The probehead shown is a double resonance $^3H/^1H$ devised by Phoenix NMR (https://phoenixnmr.com/).**

Funded by the European Union

## 2.2 NMR of tritiated solids

In liquids, most of NMR interactions are averaged out by the Brownian motion, yielding narrow peaks at frequencies given by the isotropic chemical shift values only that can be easily related to their chemical speciation. In solids, the standard approach is to work with *samples in powder form*. Then, for each orientation of crystallite with respect to the external magnetic field, the NMR shift varies (due to the anisotropy of the NMR interactions) yielding a so-called (broad) powder NMR spectrum. Depending on the strength of the anisotropy of the NMR interactions, the width of the spectrum can hamper the resolution of the various atomic species. The standard technique for improving the resolution is the *sample rotation at the magic angle* (magic-angle spinning or MAS NMR). The sample rotates around an axis oriented at the so-called magic-angle (54.72°) with respect to the external magnetic field $B_0$. In practice, the sample is packed in *powder form* in a rotor, a cylinder made of a hard ceramic, typically $ZrO_2$ or $Si_3N_4$, as shown in Figure 8d. The rotor spins in the RF coil (i.e., the antenna used for both excitation and detection of the NMR signal) at a frequency of several kHz (typically from 2 to 20 kHz with our commercial probes). The sample rotation is controlled by two gas flows: the bearing gas that stabilizes the axis of rotation of the rotor, and the drive gas that controls the spin rate (using a spinning cap shaped with winglets), as shown in Figure 9. Pressure of bearing and driving gas are *permanently* controlled by a pneumatic MAS unit using an *optical detection system* of the spin rate in order to ensure the stability of the sample rotation. The spinning gas generates an exhaust flow of about 10 to 20 l/min that can be useful to limit the accumulation of contamination if tritiated gas release occurs.

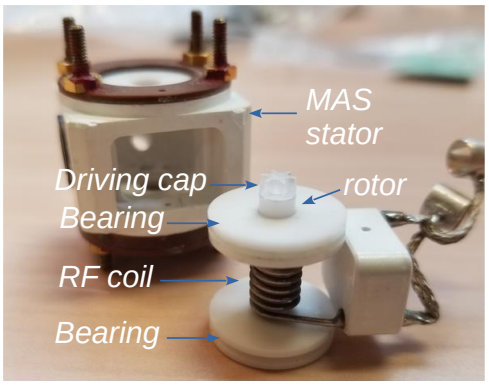


**Figure 9. (Left) View of a disassembled MAS stator showing the RF coil and the spinning system (bearing and driving).**

The main risk of dissemination comes from a sudden instability of the sample rotation that may stop the spinning (in the best case), damages the RF coil (shown in Figure 9), or - in the worst case - cause the explosion of the

rotor (*rotor crash*). In this case, this can lead to the dispersion of the samples in the probe and in the magnet. Therefore, a spinning exhaust gas system must be devised in order to ensure the confinement of the exhaust spinning gas to a tritium bubbler before the external outflow (as shown in Figure 8b). Other approaches has been devised for ensuring the confinement of a spinning radioactive sample, such as the full nuclearization of the NMR probehead (confined in a glove box under the magnet) [4] or a reinforced conditioning inside the rotor (double barrier) [5]. In the case of a non-spinning sample (referred to as *static* NMR experiment), the MAS NMR probehead can be used but the sample can then be sealed in a glass tube of adequate outer diameter. In our lab, we use Pyrex® glass tube that are flame-sealed. Particular care must be paid when centering the sample so that it is positioned in the RF coil, as illustrated in Figure 10.

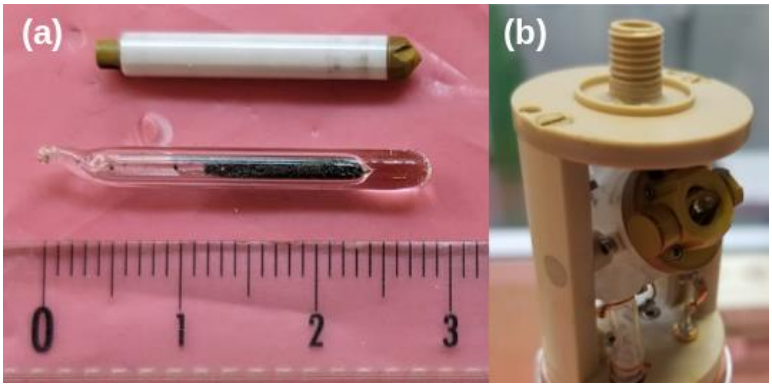


**Figure 10. For static NMR experiments (i.e., non-spinning sample); sample are packed in a glass tube (flamed sealed) with dimensions close to a MAS rotor (here 3.2mm outer diameter). The sample must be well-centered in order to be in the RF coil (see Figure 9).**

NMR Experiments are conducted in a non-nuclearized NMR laboratory (CEA Paris-Saclay, IRAMIS/NIMBE, see general view in Figure 8a) using a commercial NMR spectrometer (Bruker Avance IV neo) but with dedicated $^{3}$H MAS NMR probeheads. We possess a double resonance $^{3}$H/$^{1}$H 3.2mm MAS NMR from Phoenix NMR (https://phoenixnmr.com/) shown in Figure 8 and a triple resonance $^{3}$H/$^{1}$H/X 4mm MAS NMR probe from DOTY scientific (https://dotynmr.com/). Note that $^{3}$H (as well as $^{3}$He) are non-standard nuclei for standard commercial configuration of solid-state NMR spectrometer and thus necessitates specific additional RF equipements. Specific activity of tritiated samples is limited to few tens of mCi (per sample). From previous studies, it was determined that ~10 mCi was largely sufficient to get good a signal/ratio, in the case of model samples with *chemically bound tritium* atom in organic molecules [6] or on the surface of nanodiamond [7]. We are therefore working in *two stages*. In the first stage, powder samples are conditioned in a glass tube for performing the first *static* NMR experiments (validation of the samples, comparison of sensitivity between the probeheads which implements a different RF design). For the second stage,

samples will be conditioned in rotors (work in progress) for high-resolution MAS NMR experiments.

## 2.3 Short review of $^{3}H$ NMR in Solids

In recent years, only a very limited of studies using $^{3}H$ MAS NMR have been reported in the literature, whereas the use of $^{3}H$ in organic chemistry (NMR in liquid state) is less restricted and has been reviewed recently [8]. In solids, we can cite the seminal work Bowman et al. who investigated the ageing of palladium tritides with NMR of helium-3 and tritium. Variations of the $^{3}He$ and $^{3}H$ NMR relaxation times ($T_1$ and $T_2$) with the temperature were used to determine the speciation of helium (forming pressurized nanobubbles) and tritium (found to be located at the surface of the nanobubbles)[9]. We have investigated similar systems recently at high magnetic field (7T)[10]. In the work of Yuen et al.,[6] we performed the first MAS NMR study of tritiated organic molecules. It could be demonstrated that $^{3}H$ MAS NMR provides excellent spectral resolution (that cannot be reached for $^{1}H$) and sensitivity for longe-range interatomic ($^{3}H$-$^{3}H$) distance measurements (up to 14Å). Recently, surface of nanodiamond were investigated by $^{3}H$ and $^{2}H$ NMR showing the effective formation of C-H bonds on the surface[6]. Spectra displayed in Figure 11 show that $^{2}H$, $^{3}H$ (and thus $^{1}H$) isotropic chemical shifts are identical, and the gain in spectral resolution provided by MAS NMR (vs non-spinning sample). A recent NMR study of tritium in $LiAlO_2$ ceramic resulting from the neutron capture by lithium (through the reaction $Li^{6}$ + neutron becomes $He^{4}$ + tritium) is also illustrative of the potential of $^{3}H$ NMR (without MAS)[11].

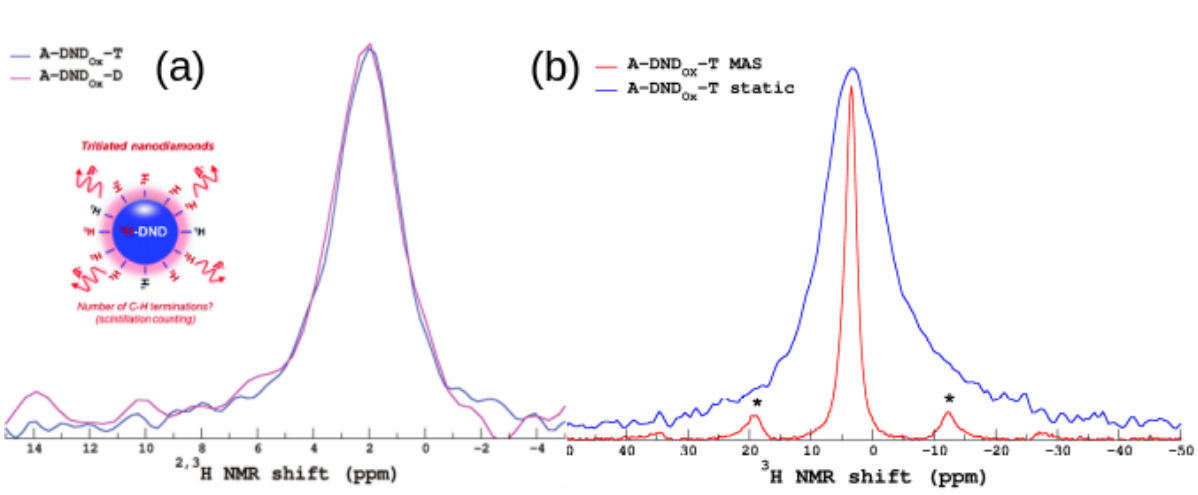


**Figure 11. (a) Comparison between $^{3}H$ and $^{2}H$ MAS NMR spectra of tritiated and deuterated nanondiamond showing formation of C-H bonds. (b) Comparison between $^{3}H$ static (i.e., non-spinning) and MAS NMR spectra if tritiated nanodiamond (*: spinning sidebands). Spectra are normalized to the same height. Data from Ref [7]. Data were acquired with the DOTY XC4 MAS NMR probe.**

## 2.4 Samples

Tritiated waste materials from nuclear plants (available in CEA Paris-Saclay) could not be used as being contaminated with other radionuclides that are not authorized in CEA solid-state NMR laboratory. Tritiated samples were therefore prepared in collaboration with M. Payet (CEA Paris-Saclay, IRFM) at the Tritium facility of CEA-Paris Saclay (CEA-JOLIOT/SCBM). Two representative systems were chosen: i) a Portland type cement CEM-I; ii) a magnesium potassium phosphate cement (MKPc) currently studied in our lab (Arthur Listwan, PhD thesis, 2021-2024) in the context of tritium wastes conditioning. Materials in powder form were tritiated under 400 mbar of $T_2$ from 2h to 18h. A tritium gas release was observed during several months and their transfer to the NMR lab was therefore delayed. The list of the prepared samples for the *static* NMR experiments is given in Table 2.

| SAMPLE | Compound | $^3$H Activity MBq/mg | Mass (mg) | Preparation |
|---|---|---|---|---|
| **MP-2109-PC02** | CEM-I cement | ≤ 2.06 | 14 | 18h $T_2$ at 400 mbar |
| **MP-2307-MKP01** | MKP cement with Mn/$Ag_2O$ getter | ≤ 1.36 | 22 | 18h $T_2$ at 400 mbar |
| **2306-MKPs-2h** | MKP cement | ≤ 5 | 20 | 2h $T_2$ at 400 mbar |
| **2306-MKPp-18h** | MKP cement with Mn/$Ag_2O$ getter | ≤ 5 | 20 | 18h $T_2$ at 400 mbar |

**Table 2. List of prepared samples for $^3$H NMR experiments, conditioned in 3mm o.d. flamed-sealed pyrex tube for static (i.e. non-spinning samples) NMR experiments.**

## 2.5 Results

NMR experiments had first to be optimized for the observation of the very short NMR signal under static conditions, as illustrated in Figure 12a. A spin-echo pulse sequence was performed in order to delay the signal. Typically, for tens of MBq, the experimental for a spectrum with a reasonable signal to noise ratio was ranging from 5h to 10h (number of scans from 8k to 16k), as shown in Figure 12b. Figure 13a shows the $^3$H NMR spectra of the MKP cements acquired under identical conditions, with (2306-MKPs-18h) and without tritium getter (2306-MKPs-2h), respectively. No signal is detected with tritium getters, as also observed for MP-2307-MKP01 (data not shown), despite similar level of contamination. These preliminary results suggest that $^3$H trapped in getter is invisible to NMR ($Mn^{4+}$ is paramagnetic and

Funded by the European Union

causes such a significant broadening of the spectrum that is vanishes). Longer experiments needs to be carried out as initial results shows the long relaxation time ($T_1$) of $^3H$ (Figure 13b).

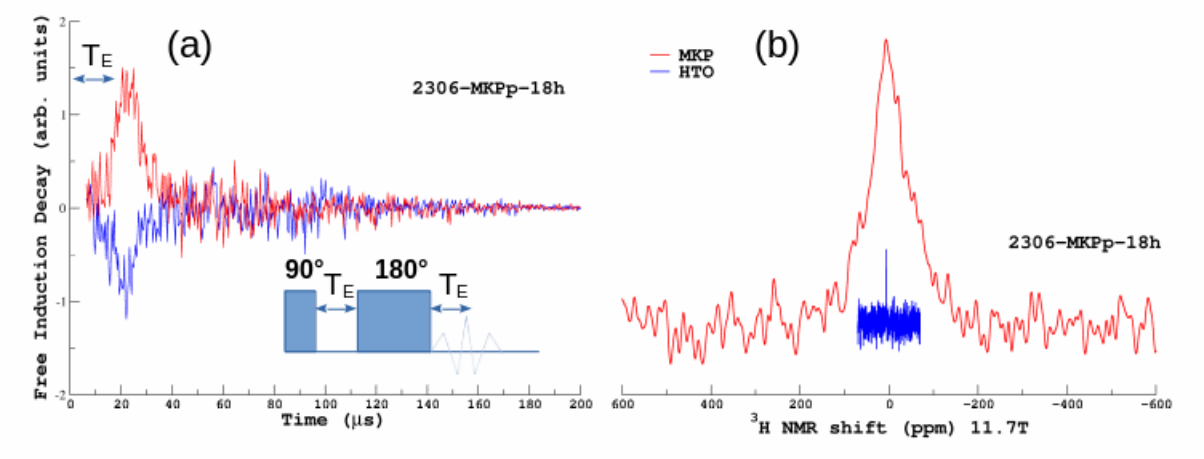


**Figure 12. NMR experiments in static conditions (i.e. non spinning) of sample tritiated MKP cement 2306-MKPp-18h (see Table 2**¡Error! No se encuentra el origen de la referencia.**) (a) Free induction decay (FID) obtained with a spin echo RF pulse sequence (echo delay $T_E$=20 µs); number of scans 8192, recycle delay 2s (experimental time 4h30). (b) NMR spectrum. Tritium NMR shift is referenced relative to HTO at 5 ppm.**

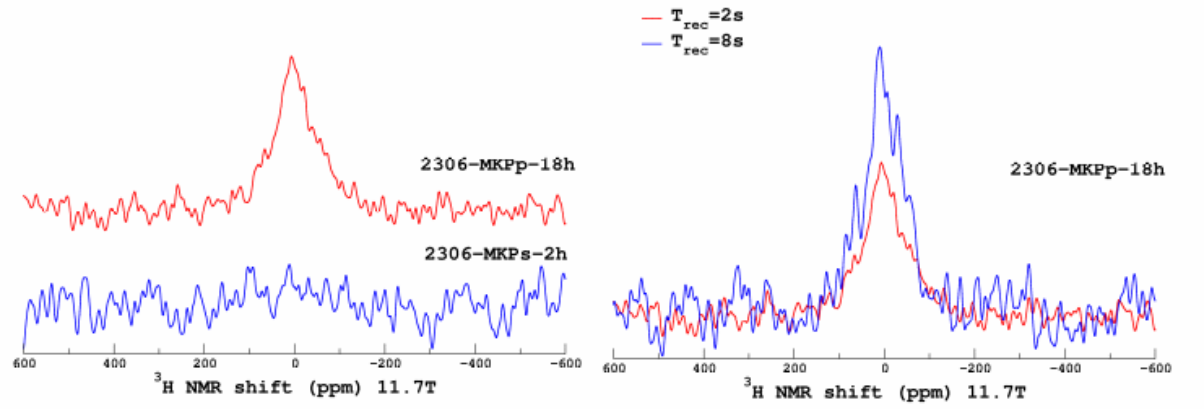


**Figure 13. (a) Comparison between $^3H$ NMR spectra of MKP cements without (2306-MKPp-18h) and with (2306-MKPs-2h) tritium getters ($MnO_2$/$Ag_2O$). (b) Example of variation of the $^3H$ NMR spectra with the recycle delay (delay between two scans) showing that longitudinal relaxation time $T_1$ is of the order of seconds (not yet determined, in progress). Spectra are normalized to the same number of scans.**

Figure 14a shows that the NMR spectrum is not impacted by $^1H$ RF decoupling (continuous RF irradiation of $^1H$ at high power during the $^3H$ signal acquisition in order to cancel out $^3H$-$^1H$ magnetic dipolar interactions), suggesting the presence of $^3H$ in gas form in the cement. In contrast for the CEM-I sample (Figure 14b), the $^1H$ RF decoupling effectively improves the resolution and sensitivity, in addition to a much narrower spectrum versus

MKP cement. Thus, the speciation of the tritium in both materials seems to be different, and deserve further studies.

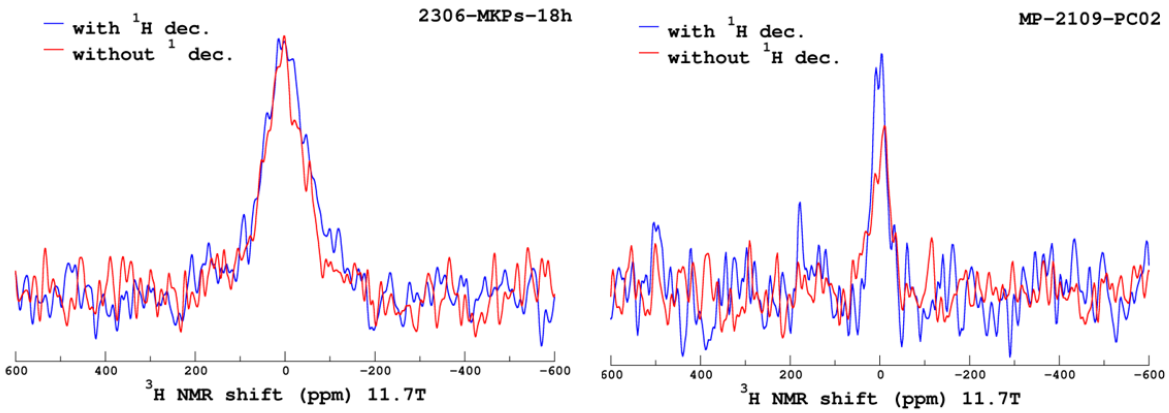


**Figure 14. Impact of the proton decoupling on the $^{3}H$ spectra of a (left) MKP cement and a (right) CEM-I cement. Spectra are normalized to the same number of scans.**

## 2.6 Conclusion and perspectives

In conclusion, first tritium NMR experiments were carried out with representative cementitious materials with a tritium activity of the order of MBq/mg and a sample mass of 20mg. NMR signals could be acquired in few hours with a reasonable signal to noise ratio at magnetic field 11.7T. More advanced techniques such as $^{1}H$ to $^{3}H$ cross polarization (transfer of magnetization from $^{1}H$ to $^{3}H$)[6] must be investigated for further gain in sensitivity. More NMR experiments will carry out on samples from Table 2. to extract important NMR parameters ($T_1$, $T_2$, NMR linewidth and shift), as such data have never been reported in the literature to the best of knowledge.
As illustrated in Figure 11b, a significant gain in resolution and sensitivity can be expected using MAS NMR (the spectrum aera is constant and thus its narrowing results in an increase of the signal to noise ratio). Procedure for filling MAS NMR rotors (see tools in Figure 15a) is currently examined. Once filled, the rotors will be assessed using a spinner bench (see Figure 15b) before their transfer to the CEA solid-state NMR from the CEA tritium lab.

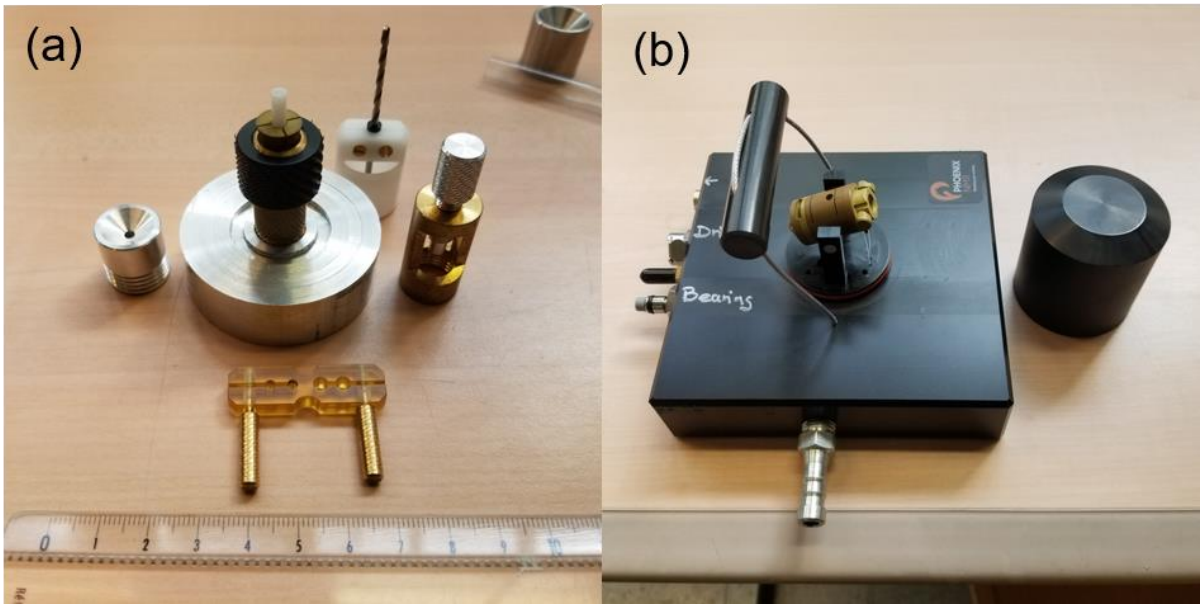


**Figure 15. (a) Tools for the filling of MAS NMR rotors. (b) Spinner bench used for testing the stability the rotor rotation in the CEA tritium laboratory before its transfer to the CEA NMR lab.**

# 3 Tritium measurement in tritiated solids by nuclear reaction analysis

Ion beam methods are among the few techniques that can detect hydrogen isotopes [12], so they are often used for post-mortem analysis of samples exposed to fuel in fusion devices [13]. There are also other methods such as the accelerator mass spectrometry (AMS) and full combustion method (FCM), which can provide quantitative tritium profiles and are proven to have better detection sensitivity compared to ion beam analysis methods [14]. In addition, chemical etching and subsequent analysis of tritium in the etching solution by liquid scintillation counting can also provide quantitative tritium depth profiling [15][16]. These methods were successfully used to determine very low levels of tritium in samples exposed in the JET fusion device [15][14] and gave very valuable information on the tritium retention. However, it must be emphasised that all these methods are destructive, whereas ion beam methods are in most cases non-destructive.

Nuclear reaction analysis (NRA) method is typically used for samples with small amounts of hydrogen isotopes due to its high sensitivity [17] and its insensitivity to sample surface roughness and contamination [18][19]. The purpose of this study was to evaluate the cross-section for the nuclear reaction between tritium and $^{3}He$ and use it for analysis of thick solid

samples. In the literature one can find that $^{3}He$ induces nuclear reactions with tritium, via at least three reaction channels [20][21][22]:

$$^{3}H + ^{3}He \rightarrow ^{4}He + ^{2}H + 14.32\ MeV \quad (1)$$
$$\rightarrow ^{4}He + ^{1}H + n + 12.09\ MeV \quad (2)$$
$$\rightarrow ^{5}He + ^{1}H + 11.36\ MeV \quad (3)$$
$$^{5}He \rightarrow ^{4}He + n + 0.73\ MeV$$

The advantage of using $^{3}He$ as the primary beam for tritium concentration measurements is that it would allow the detection of tritium simultaneously with deuterium [23][24] and other impurities that are typically present in fission and, especially, fusion environment such as carbon, oxygen, boron and beryllium. This is important for post-mortem analysis of samples and tiles exposed in fusion devices such as JET and future fusion devices like ITER and DEMO.

We have started to measure the differential cross-sections for two decay channels for the nuclear reaction between $^{3}He$ and $^{3}H$ in the energy range between 0.6 MeV and 3.4 MeV within the scope of TRANSAT project and within the TITANS project the cross sections were evaluated. The cross-sections were measured at three different scattering angles 125, 135 and 155°. The evaluated cross-section was compared with the cross-section determined by Nocken et al. [21], Kuhn et al. [20] and Nam et al. [25] and good agreement was found with the present measured cross-section.

## 3.1 Sample preparation

In our last publication [26], a thick solid tritiated W sample was produced in order to probe the efficiency of tritium detection with a $^{3}He$ ion beam using NRA. Due to the very low signal at individual 3He energies, the quantification of the differential cross-section was not possible in this first attempt [26]. For proper quantification, a more pronounced and better separation of the two peaks coming from the $^{3}H(^{3}He,d)^{4}He$ and $^{3}H(^{3}He,p)^{5}He$ channels should be achieved. This could be achieved by using a thinner target with a much higher tritium concentration. Such requirements were achieved by using a PdTi thin layer film deposited on a Si wafer. The sample was prepared by depositing thin layers of Ti and Pd by a triode sputtering device on a 0.25 mm thick Si (100) wafer at Jozef Stefan Institute (JSI). We have chosen for this material composition since is well-known that Ti is a hydrogen getter[27]. The use of Pd was decided due to the fact that Pd acts as a catalyst for hydrogen molecule dissociation on the surface and can prevent Ti oxidation [28]. The individual layer thicknesses were determined with the Rutherford backscattering spectroscopy measurements. The PdTi layer consisted of $(115 \pm 6)\times10^{15}$ Pd atoms/cm$^2$ corresponding to 17 nm of Pd on top of $(335\pm10)\times10^{15}$ Ti atoms/cm$^2$ corresponding to approximately 59 nm of Ti, deposited on a Si wafer.
A successful loading procedure was developed with deuterium gas at $1.8\times10^{5}$ Pa at different temperatures of 200°C, 300°C and 400°C. The success of the loading procedure was tested by the $^{3}He$ NRA method at the JSI. The

trapping of deuterium was successful at all temperatures. The protocol that is used is divided into two steps. In the first step, the sample is exposed to $^{1}H_2$ atmosphere (99.9992%) at 300±2 °C and (1.55 ± 0.05)×$10^5$ Pa. During this step, the uptake of hydrogen into the titanium bulk is initialized. The palladium promotes the hydrogen uptake on titanium preventing and limiting the formation of titanium oxide acting like a barrier for hydrogen isotope absorption. Moreover, traces of water are removed thanks to a $CO_2$ cold trap at -79.5°C. In the second step, the sample is exposed to the labelling isotope ($^{2}H_2$ or $^{3}H_2$ at 99% of isotopic enrichment) gas atmosphere in a sealed glass tube. The treatment lasts 1 hour at 300±2°C and above (1.55 ± 0.05)×$10^5$ Pa. According to the protocol, two fresh samples were loaded with $^{3}H_2$ gas at 300 °C and 1.6×$10^5$ Pa for 1 hour. The sample is placed in an airtight container and is swept by the non-contaminated airflow. Tritium release from the sample is then trapped in the feeding bottles of a tritium bubbler (MARC 7000 from SDEC France 2010). As, tritium release was detected at room temperature after many days, an annealing procedure was performed: the sample was heated to 100°C to remove the loosely bound tritium that would migrate at room temperature and to guarantee zero release of tritium during transport and NRA experiments. One of the two samples was sent to JSI for cross-section analysis. The second one was used to determine the total $^{3}H$ activity by liquid scintillation counting technique using a Tri-Carb 2910TR analyser from Perkin-Elmer. The coupling of the heating system with the airtight tank and the bubbler allows forced outgassing of tritium from the sample. The total activity is accumulated in the bubbler after a 4h step at 200 °C and measured by liquid scintillation. Another step followed with an increasing temperature from 200°C to 800°C to control the end of the release. Tritium release was checked by rapid annealing to 1000°C and no increase in release activity was observed. After 15 hours of cooling down (the furnace temperature decreases slowly), there was still no increase in the release activity from the sample. Finally, the sample was checked with a surface contamination meter (LB123 from Berthold Technologies). The intensity of the signal was less than two times the background noise. This means sufficiently low to neglect a small amount that could be trapped in the sample compared to the uncertainty of the measurements. The total amount of tritium activity measured after such procedure was 270 MBq for a sample with an area of 53.3 $mm^2$ which leads to 395 ± 59 MBq for a sample with an area of 77.96 $mm^2$ (11.3 × 6.9 $mm^2$) studied by NRA.

## 3.2 Cross section determination

The obtained differential cross-sections measured at 135° determined individually for the channel (1) denoted as "$^{4}$He+d" and channel (3) denoted as "$^{5}$He+p" are shown in Figure 1. We compare also the cross-sections measured by Kuhn et al. [20], Nocken et al. [21] and Nam et al. [25]. In the energy range where we have some overlap with the present study, we have

excellent agreement with Kuhn et al. and very good agreement with the other two literature data. The data by Nam et al. are slightly higher than the present data, but it needs to be noted that the scattering angle in that case was 132° ± 1° except for the data point for the lowest energy. In the case of ref. [25] it was measured at 138° and this data point is slightly lower than our data. This indicates that there might be a strong angular dependence, which will be shown in the following.

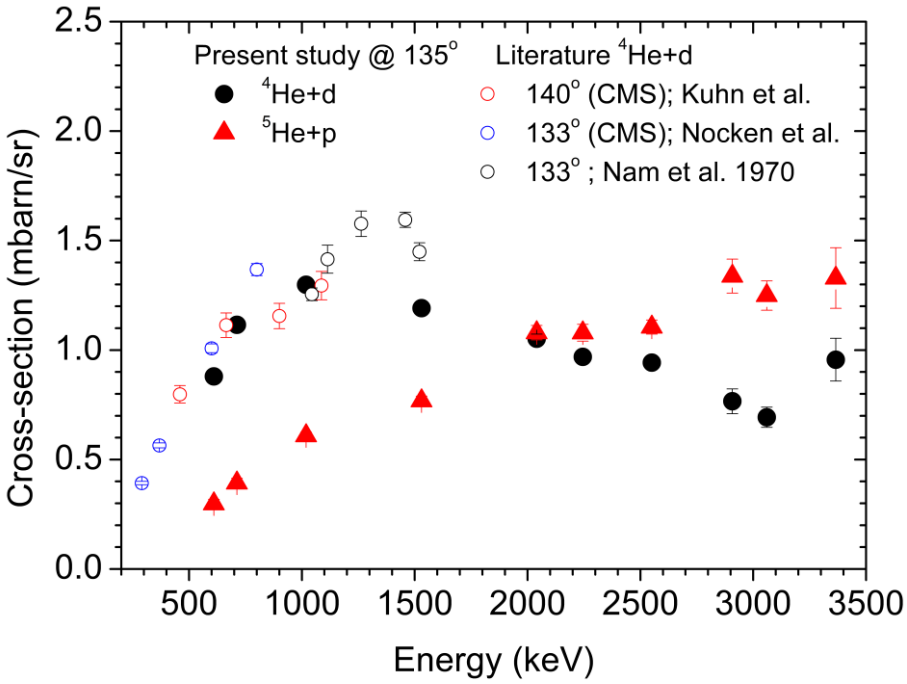


**Figure 16: Differential cross-sections determined at the scattering angle of 135o separately for channel (1), marked as "4He+d", and channel (3), marked as "5He+p". For comparison we also show the cross-sections measured by Kuhn et al. [20] , Nocken et al. [21] and Nam et al. [25].**

## 3.3 Tritium determination in thick solid target

The differential cross-sections measured at 135° were verified on a thick tritiated solid tungsten target. For this purpose, a tungsten sample was first irradiated by 20 MeV W ions to create defects into which hydrogen isotope atoms can be trapped, as described in [26][29]. The sample was loaded at 450°C by $^{3}H_2$ gas. The sample loading and measurement procedure is described in detail in [26]. The applied $^{3}$He beam analysing dose was 34.2μC for energies ≤ 2500 keV and 17.1 μC for energies > 2500 keV, which is four times higher dose than that used for the PdTi film. No outgassing during $^{3}$He analysis is anticipated since deuterium is strongly trapped at defects in tungsten [30]. At most 6% reduction of deuterium was measured on such samples after 1.5 years [31]. The experimental spectra obtained on that sample were then fitted in the SIMNRA program [32] using the above-determined differential cross-sections at 135° by varying the tritium depth profile in the target. The obtained fits are shown in Figure 17 for different $^{3}$He

energies. The tritium depth profile that gave the best fit to the spectra is shown in Figure 18. With such a depth profile we managed to obtain a good agreement of the integral counts and the shape for the first narrow peak from reaction channel $^{3}H(^{3}He,d)^{4}He$, for all energies. The different energies give information about the tritium depth profile at different depths. Namely, at higher $^{3}He$ energies we obtain the information from higher depths since the penetration of the beam is deeper.

We show in the Figure 17 also the SIMNRA fitting result for the channel (3) which is $^{3}H(^{3}He,p)^{5}He$. Contrary to the first one, the simulated right peak is not in good agreement with the measured spectra. This is mainly due to the fact that the resonance for this decay channel is very broad and therefore the energy distribution of the products is also broad. This means that the protons coming from that reaction have a larger energy distribution than is usually given from nuclear reaction channels. For this reason, the right peak was broadened by the width of the reaction and is shown additionally as a dashed line for individual energies. The sum of the first peak and the width-corrected peak is shown as a black line. The agreement of the corrected simulated spectra and the measurement is then very good.

Since we can still rather well distinguish the contribution from the two decay channels, we were able to determine the tritium depth profile by fitting the first peak from the channel (1). The $^{3}H$ depth shown in figure 2.3 is compared to the $^{2}H$ depth profile obtained on a sample that was loaded by $^{2}H_{2}$ gas in the same way as the tritiated sample. Both samples were irradiated by 20 MeV W ions that create displacement damage down to 2.3 μm where hydrogen isotopes are effectively trapped. The $^{2}H$ and $^{3}H$ concentrations are in good agreement within this damaged depth, showing a homogeneous $^{2}H$ and $^{3}H$ concentration of 0.20 at. % for $^{3}H$ and 0.25 at. % for $^{2}H$ from 0.2 μm down to 2 μm. The tritiated sample beyond 2 μm attains 0.12 at. % down to 3.6 μm and then decreases to 0.001 at. % which is the level that we typically observe on unirradiated polycrystalline W. The difference between $^{3}H$ and $^{2}H$ concentrations in this second layer from 2 to 3.6 μm could be due to the poorer depth resolution for $^{3}H$ or the uncertainty in the signal fit due to the background from channels (2) and (3), which becomes higher at higher $^{3}He$ energies. The $^{3}H$ concentration below 3 μm is not easy to determine since an overlap exists with the signal from the channel (3). Since the cross-section for the channel (1) has no sharp resonance and is almost constant over the measured energy range, this means that we are similarly sensitive at all analysing depths. Therefore, the distribution of the measured signal at a given energy gives us the informative distribution of the tritium in the sample. Varying the energy only changes the depth to which we can still obtain information about the $^{3}H$ concentration. Therefore, by measuring at 2.5 MeV beam energy, we obtain information about the amount of $^{3}H$ down to about 3.5 μm. Measurements at higher energies will not give us with any additional information because the signal from higher depths is in the energy range where we have an overlap with the signal from the channel (3) and therefore we cannot determine the $^{3}H$ concentration with high accuracy.

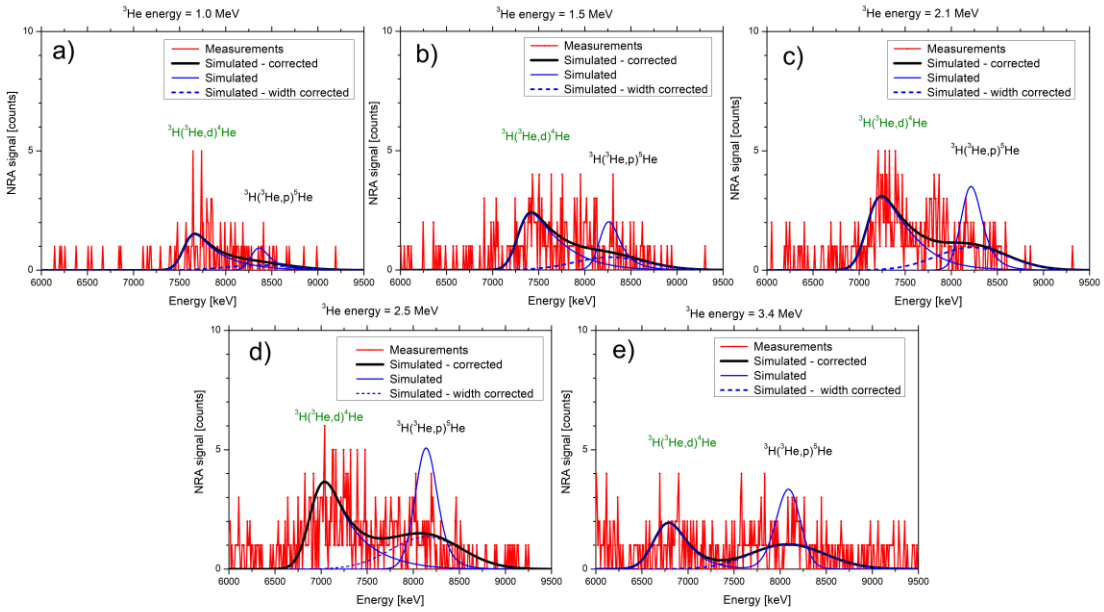


**Figure 17: Experimental spectra (red) measured at different primary 3He ion energy from 1 MeV to 3.4 MeV at 135o together with the fitted spectrum (black) using the above determined differential cross-sections. The simulated spectra as obtained from SIMNRA (blue line), was for channel (3) corrected for the width of the reaction channel and is shown as a dashed blue line. This width-corrected spectrum is then summed together with the spectrum for channel (1), shown as a black line.**

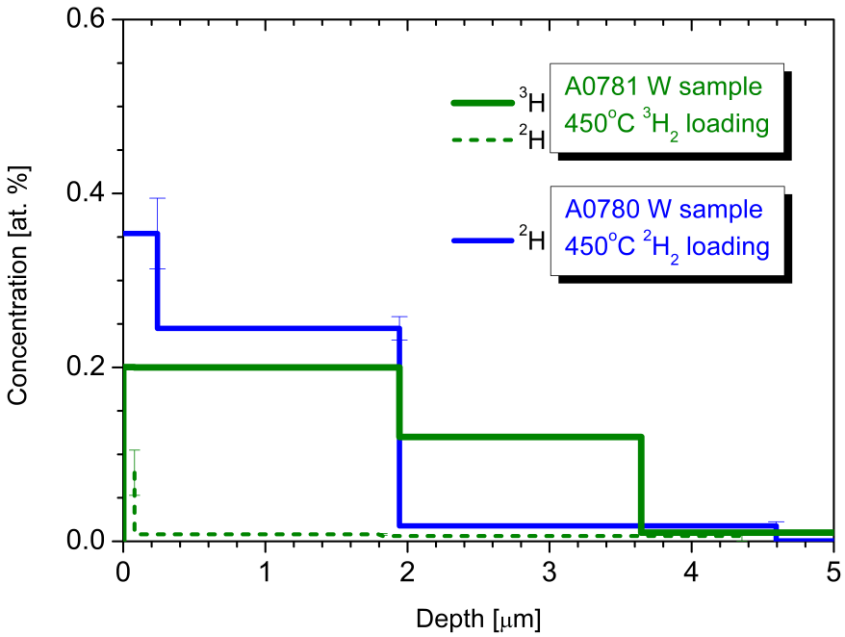


**Figure 18: The $^{3}H$ depth profile for the W self-damaged sample A0781 exposed to $^{3}H2$ gas at 450°C, olive line. This depth profile was used for the fitting of the spectra shown in figure 2. Dashed green shows the $^{2}H$ concentration in this sample. For comparison we also show the 2H depth profile as obtained on the W self-damaged sample A0780 exposed to 2H2 gas at 450oC, blue line.**

## 3.4 Conclusion on the use of NRA for tritium measurement for solid targets

We have measured and evaluated differential cross-sections for two decay channels for the nuclear reaction between $^{3}He$ and $^{3}H$ in the energy range between 0.6 MeV and 3.4 MeV. The cross-sections were measured at three different scattering angles 125, 135 and 155°. The evaluated cross-section was compared with the cross-section determined by Nocken et al. [21], Kuhn et al.[20] and Nam et al. [25] and good agreement was found with the present measured cross-section. With the obtained cross-sections we have evaluated the $^{3}H$ depth profile on a thick tungsten target measured in [26]. We have fitted the measured spectra for the channel (1) by changing the $^{3}H$ distribution in the sample. The obtained $^{3}H$ depth profile is in good agreement with the deuterium depth profile on a sample that experienced the same irradiation and loading procedure, but with a $^{2}H_2$ exposure gas. We estimated that with the present differential cross-section data we can obtain $^{3}H$ depth profile information down to 3.5 µm in tungsten. Beyond this depth, the signal from the channel (1) overlaps with the signal from the channel (3), which has a broad energy distribution and cannot give us reliable information about the $^{3}H$ depth profile. The above presented results were published in Journal Nuclear Material and Energy https://doi.org/10.1016/j.nme.2024.101586 .

# 4 Tritium measurement in a tritiated aerosol by LIBS

## 4.1 Choice of the experimental conditions

The measurement of the composition of aerosols has already been carried out previously by LIBS (Laser-Induced Breakdown Spectroscopy). We recall that this technique consists of forming, after focusing using a lens a nanosecond laser pulse at sufficiently high energy, a thermal plasma on the material to be analysed. Following this irradiation, the thermal plasma is hot enough to emit a spectrum whose spectroscopic analysis allows us to trace the composition. This observation must be carried out under conditions of Local Thermodynamic Equilibrium (LTE) in order to allow the complete reconstruction of this spectrum. To ensure the LTE conditions, a background gas such as helium or argon can be used at atmospheric pressure or at 50% of this level.
Calculations were carried out in order to establish the mole fraction threshold from which the observation of the Hα line (one of the Balmer series, main transition of hydrogen isotopes observable in the visible

spectral range) is possible in the spectrum, among the transitions other species present and those of the background gas. As laser-induced plasmas produced in helium are hotter at short times, which allows a reduction in the observation and quantification limit, we decided to use this gas as a background gas. Given previous experience at IRSN with alumina powder, $Al_2O_3$ will be used. Starting from a maximum tritium concentration of around 100 GBq/g, it is necessary to obtain a $C_m$ concentration of approximately 1000 mg/m$^3$ of powder in suspension to hope to observe a satisfactory level signal level.

## 4.2 Aerosol production

Such a concentration can be obtained by using a Vortex Shaker (see figure 1) equipped with bronze balls at its base and powders to be suspended. This system was implemented and tested with a view to its coupling with the rest of the device. Its characterization was carried out under helium with alumina particles. These were measured from the point of view of their diameter distribution at the exit of the vortex using an optical particle size analyser.

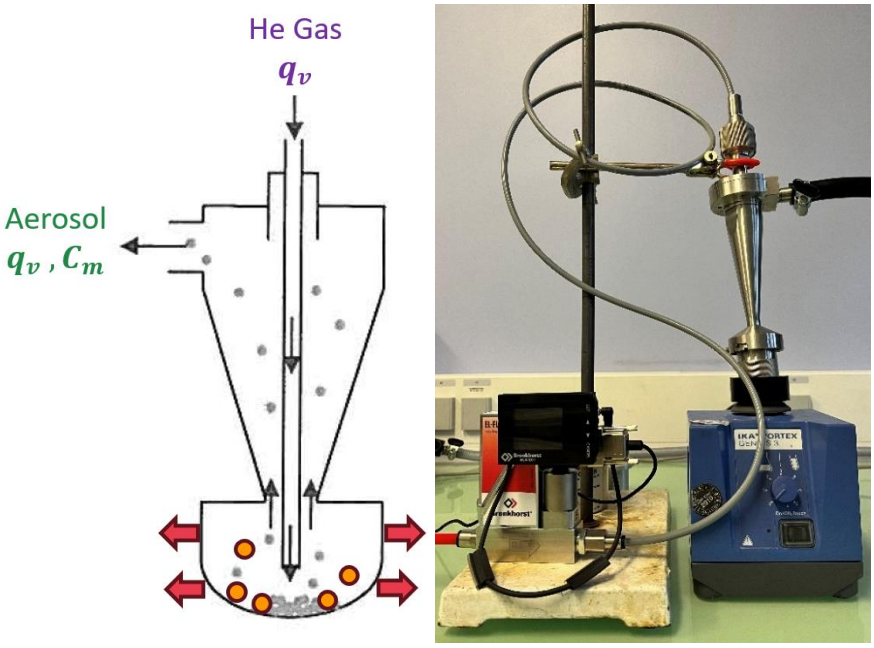


**Figure 19: Left: principal of the Vortex Shaker. Right: implementation and tests.**

## 4.3 Aerosol flow modelling

The use of helium and laser irradiation require the use of portholes to isolate everything from the outside. These windows must be placed relatively far from where the particles are present and at the same time close to them in order to allow the intense focusing of the laser light by the lens. These apparently contradictory conditions can be obtained by the use of guide nozzles making it possible to obtain a highly collimated jet loaded with particles, with two side chambers avoiding the injection of particles and making it possible not to dirty the portholes through which the laser irradiation is carried out. The whole thus forms a cross. Figure 2 shows the maps calculated with OpenFOAM based on an axisymmetric RANS simulation under these conditions.

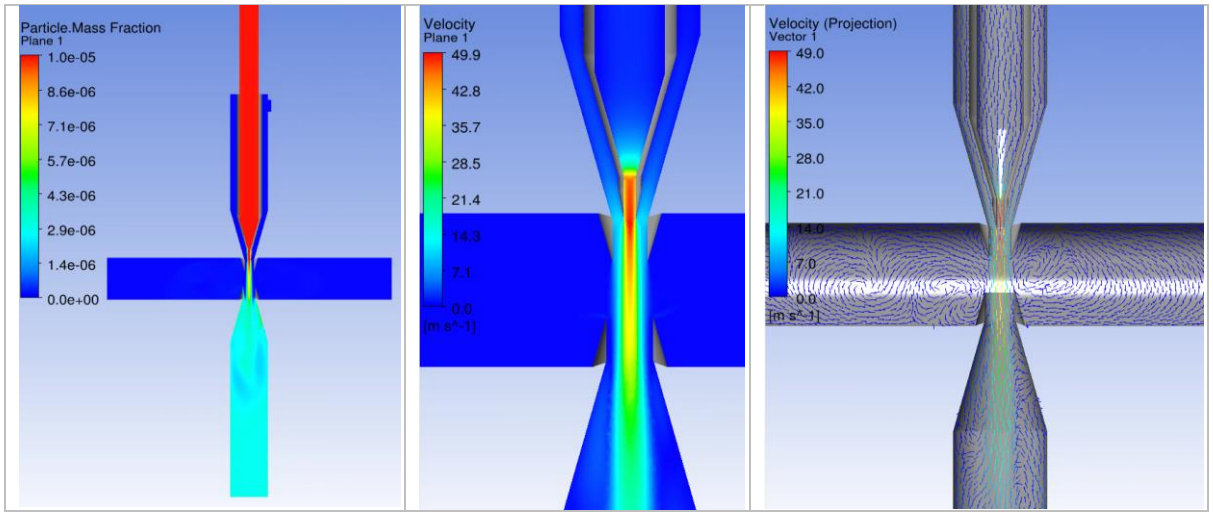

| | | |
|---|---|---|
| (a) Particule mass fraction | (b) Velocity | (c) Velocity projection |

**Figure 20: Modelling of the flow charged with particles within the pipes for the LIBS experiment from an axisymmetric RANS approach using OpenFOAM.**

These modelling results made it possible to choose the most favourable geometric conditions and dimensions.

## 4.4 The LIBS chamber

Following the determination of the optimal flow conditions, the choice of nozzles was made. They are currently being produced, in accordance with Figure 21.

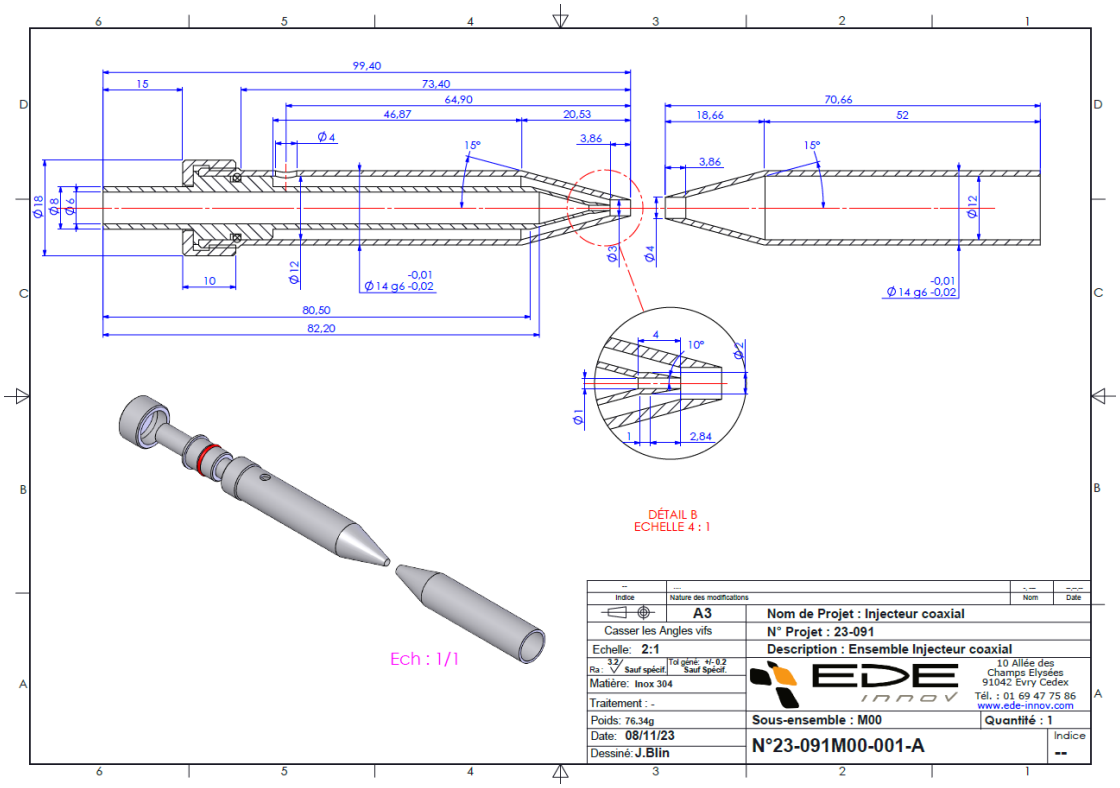


**Figure 21: Design of the nozzle preparing the aerosol flow for the LIBS experiment at the center.**

The whole will be positioned in the center of a chamber (see figure 4) equipped with windows allowing laser irradiation.

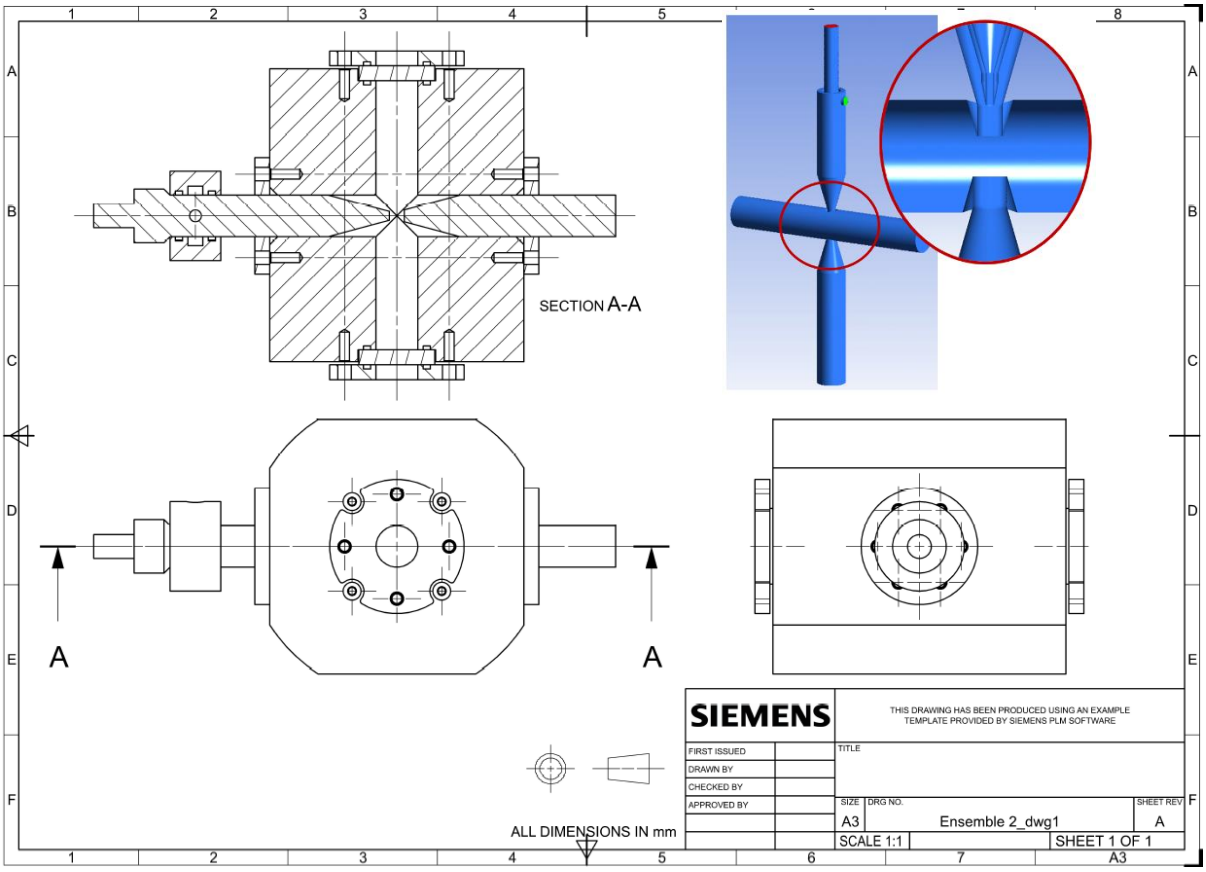


**Figure 22: Design of the experimental chamber receiving the nozzle of figure 3.**

This experimental chamber is currently under construction.

# Conclusion

The advancements in tritium measurement techniques presented in this document highlight significant progress in the field. Each method—autoradiography, NMR, NRA, and LIBS—offers unique advantages and applications, contributing to a comprehensive toolkit for tritium analysis. Continued research and development in these areas will be crucial for improving the precision, sensitivity, and applicability of tritium measurement techniques, ultimately aiding in the safe handling and monitoring of tritium in nuclear and environmental contexts.

Funded by the European Union

# 5 Bibliography

[1] M. J. Duer, Introduction to Solid-State NMR Spectroscopy., Wiley., 2005.
[2] Levitt, M. H. Spin Dynamics: Basics of Nuclear Magnetic Resonance (2ed.). Wiley. 2008
[3] MacKenzie, K. J. D., & Smith, M. E. Multinuclear solid-state NMR of inorganic materials. Elsevier. 2002
[4] Martel, L. A nuclear magnetic resonance spectrometer concept for hermetically sealed magic angle spinning investigations on highly toxic, radiotoxic, or air sensitive materials. Review of Scientific Instruments, 84(5), 055112. 2013
[5] I. Farnan, "Quantification of actinide $\alpha$-radiation damage in minerals and ceramics," Nature, vol. 445, no. 7124, p. 190 193., 2007.
[6] Yuen, A. K. L. Measurement of Long-Range Interatomic Distances by Solid-State Tritium-NMR Spectroscopy. Journal of the American Chemical Society, 132(6), 1734-1735. 2010
[7] Nehlig, E. Using hydrogen isotope incorporation as a tool to unravel the surfaces of hydrogen-treated nanodiamonds. Nanoscale, 11(16), 8027-8036. 2019
[8] Krivdin, L. B. Tritium NMR : A compilation of data and a practical guide. Magnetic Resonance in Chemistry, 61(4), 195-247. 2023
[9] R. C. Bowman, "Helium, tritium, and protium NMR studies of tritide-free aged," Physical Review B, vol. 37, no. 16, p. 9447 9454, 1988.
[10] B. Evin, "Aging of Pd under tritium: Influence of 3He generation and associated mechanisms.," Journal of Alloys and Compounds, vol. 938, p. 168589, 2023.
[11] H. Cho, "Isotope-specific analysis of neutron-irradiated lithium aluminate ceramics by nuclear magnetic resonance spectroscopy.," Journal of the American Ceramic Society, vol. 103 , no. 12, p. 7291 7298., 2020.
[12] J. Bøttiger, "A review on depth profiling of hydrogen and helium isotopes within the near-surface region of solids by use of ion beams," Journal of Nuclear Materials, vol. 78, p. 161–181, 1978.
[13] M. Rubel, D. Primetzhofer, P. Petersson, S. Charisopoulos and A. Widdowson, "Accelerator techniques and nuclear data needs for ion beam analysis of wall materials in controlled fusion devices," EPJ Techn Instrum, vol. 10, p. 1–21, 2023.
[14] C. Stan-Sion et. al., "Tritium retention measurements by accelerator mass spectrometry and full combustion of W-coated and uncoated CFC tiles from the JET divertor," Nucl. Fusion, vol. 56, p. 046015, 2016.
[15] E. Pajuste and e. al., "Structure, tritium depth profile and desorption from 'plasma-facing' beryllium materials of ITER-Like-Wall at JET," Nuclear Materials and Energy, vol. 12, p. 642–647, 2017.

[16] V. K. Alimov, Y. Torikai, Y. Hatano and T. Schwarz-Selinger, "Tritium retention in displacement-damaged tungsten exposed to deuterium-tritium gas mixture at elevated temperatures," Fusion Engineering and Design, vol. 162, p. 112100 , 2021.

[17] M. Wilde and K. Fukutani, "Hydrogen detection near surfaces and shallow interfaces with resonant nuclear reaction analysis," Surface Science Reports, vol. 69, p. 196–295, 2014.

[18] A. Jaffe, F. d. S. Barros, P. Forsyth, J. Muto, I. Taylor and S. Ramavataram, "Some (t, p) Reactions in Light Nuclei," Proc. Phys. Soc., vol. 76, p. 914–928, 1960.

[19] I. P. P. B. H. H. A. P. G. Bykov, "Investigation of tritium analysis methods for ion microbeam application," Nuclear Instruments and Methods in Physics Research Section B, vol. 273, pp. 250-253, 2012.

[20] B. Kühn and B. Schlenk, "Winkelverteilungen für die reaktion He3 + T," Nuclear Physics, vol. 48, p. 353, 1963.

[21] U. Nocken, U. Quast, A. Richter and G. Schrieder, "The reaction 3H(3He, d)4He at very low energies: Energy dependent violations of the Barshay-Temmerisospin theorem and highly excited states in 6Li.," Nuclear Physics A, vol. 213, p. 97–106, 1973.

[22] C. Moak, "A Study of the H 3+ He 3 Reactions," Physical Review, vol. 92, no. . . 92, ., p. 383, 1953.

[23] V. Alimov, M. Mayer and J. Roth, "Differential cross-section of the D(3He, p)4He nuclear reaction and depth profiling of deuterium up to large depths.," Nucl. Instr. and Meth. in Phys. Res. B, vol. 234, 2005.

[24] B. Wielunska, M. Mayer, T. Schwarz-Selinger, U. von Toussaint and J. Bauer, "Cross Section Data for the D(3He,p)4He Nuclear Reaction from 0.25 to 6MeV," Nucl. Instr. and Meth. in Phys. Res. B, vol. 371, p. 61, 2016.

[25] K. Nam, G. Osetinskii and V. Sergeev, "Isospin Conservation in the Reaction He3(t, d)He4," Soviet J. Nucl. Phys., vol. 10, p. 407, 1970.

[26] S. Markelj et al., "Tritium measurements by nuclear reaction analysis using 3He beam in the energy range between 0.7 MeV and 5.1 MeV," Nuclear Materials and Energy, vol. 28, p. 101057, 2021.

[27] Y. Fukai, The Metal-Hydrogen systems, Berlin Heidelberg: Springer-Verlag , 2005.

[28] X. Xia, W. Ding, B. Zhang, X. Long, S. Luo, S. Peng, R. Hutton and L. Shi, "Cross-section for proton–tritium scattering from 1.4 to 3.4MeV at the laboratory angle of 165°.," Nuclear Instruments and Methods in Physics Research Section B: , vol. 266, p. 705, 2008.

[29] S. Markelj, A. Založnik, T. Schwarz-Selinger, O. V. Ogorodnikova, P. Vavpetič, P. Pelicon and I. Čadež, "In situ NRA study of hydrogen isotope exchange in self-ion damaged tungsten exposed to neutral atoms," J. Nucl. Mater., vol. 469, p. 133–144, 2016.

[30] E. A. Hodille, A. Založnik, S. Markelj, T. Schwarz-Selinger, C. S. Becquart, R. Bisson and C. Grisolia, "Simulations of atomic deuterium exposure in self-damaged tungsten," Nucl. Fusion, vol. 57, p. 056002, 2017.

[31] B. Wielunska, M. Mayer, T. Schwarz-Selinger, A. E. Sand and W. Jacob, “Deuterium retention in tungsten irradiated by different ions,” Nucl. Fusion , vol. 60, p. 096002, 2020.

[32] M. Meyer, “SIMNRA User's Guide, Report IPP 9/113,” Max-Planck-Instutut für Plasmaphysik, Garching, Germany, 1997. [Online]. Available: http://www.rzg.mpg.de/~mam/.